Supplementary Information

Evoking the Dynamic Fe-N_x Active Sites through the Immobilization of Molecular Fe Catalyst on NGQDs for the Efficient Electroreduction of Nitrate to Ammonia

Mia Rinawati[1], Yen-Shuo Chiu[1], Ling-Yu Chang[1], Chia-Yu Chang[2], Wei-Nien Su[2,3], Ni Luh Wulan Septiani[3,4], Brian Yuliarto[4], Wei-Hsiang Huang[5], Jeng-Lung Chen[5], and Min-Hsin Yeh[1,3*]

[1] Department of Chemical Engineering, National Taiwan University of Science and Technology, Taipei 10607, Taiwan

[2] National Synchrotron Radiation Research Center, Hsinchu, 30076, Taiwan

[3] Research Center for Nanotechnology Systems, National Research and Innovation Agency (BRIN), Kawasan Puspiptek, Serpong, South Tangerang 15314, Indonesia

[4] Advanced Functional Materials Laboratory, Department of Engineering Physics, Institute of Technology Bandung (ITB), B233andung, 40132, Indonesia

[5] National Synchrotron Radiation Research Center, Hsinchu 30076, Taiwan

[*]Corresponding author: Tel.: +886-2-2737-6643; E-mail: mhyeh@mail.ntust.edu.tw

Table S1 Atomic composition of NGQDs and NGQDs-Fe

Electrocatalysts	XPS atomic composition (%)			
	C	O	N	Fe
NGQDs	38.7	57.9	3.4	-
NGQDs-Fe (0.1 M)	45.9	49.3	3.9	0.9
NGQDs-Fe (0.25 M)	46.6	48.2	4.8	0.4

Table S2 XPS atomic composition of the nitrogen-optimized NGQDs-Fe.

Electrocatalysts	XPS atomic composition (%)			
	C	O	Fe	N
N3-Fe	46.4	48.6	1.7	4.3
N5-Fe	51.4	41.3	1.2	6.1
N8-Fe	45.9	49.3	0.9	3.9
N10-Fe	48.8	46.7	1.1	3.4

Table S3 Nitrogen atomic composition of the optimized NGQDs-Fe

Electrocatalysts	N atomic composition (%)			
	Pyridinic N	Fe–N$_x$	Pyrrolic N	Graphitic N
N3-Fe	20.1	26.0	28.5	25.4
N5-Fe	18.9	26.8	30.7	23.6
N8-Fe	28.4	32.6	21.2	17.8
N10-Fe	21.7	27.1	28.8	22.4

Table S4 NO_3RR activity comparison of Fe catalyst reported in the literatures.

Sample	Electrolyte	Yield	Faradaic Efficiency	Ref.
Fe SAC	0.1 M K_2SO_4 +0.5 M KNO_3	20 000 $\mu g\ h^{-1}\ mg_{cat}^{-1}$	NH_3, ~75%	[1]
Fe-SAs/g-C_3N_4	0.1 M Na_2SO4 + 50 mg L^{-1} NO_3^-	–	NH_3, 98.6%	[2]
Fe SAC	0.1 M K_2SO_4 + 0.5 M KNO_3	46 mg $h^{-1}\ mg_{cat}^{-1}$	NH_3, 92%	[3]
Fe-Ppy SAC	0.1 M KOH + 0.1 M KNO_3	2.75 mg $NH_3\ h^{-1}\ cm^{-2}$	NH_3, ~100%	[4]
Ru-SAC	0.1 M KOH + 0.1 M KNO_3	0.69 mmol $h^{-1}\ cm^{-2}$	NH_3, 72.8%	[5]
Fe/Cu-HNG	1 M KOH + 0.1 M KNO_3	1.08 mmol $h^{-1}\ mg^{-1}$	NH_3, 92.51%	[6]
ISAA In-Pdene	0.5 M Na_2SO_4 + 100 mM $NaNO_3$	28.06 mg $h^{-1}\ mg_{Pd}^{-1}$	NH_3, 87.2%	[7]
Cu–N–C	0.1 M KOH + 0.1 M KNO_3	4.5 mg $cm^{-2}\ h^{-1}$	NH_3, 84.7%	[8]
Cu SAC	0.5 M Na_2SO_4 + 5 mM NO_3^-	66 μmol $h^{-1}\ cm^{-2}$	NH_3, 85.5%	[9]
NGQDs-Fe/G	0.1 M KOH + 0.1 M KNO_3	15.9 mmol $h^{-1}\ cm^{-2}$	NH_3, 93%	This work

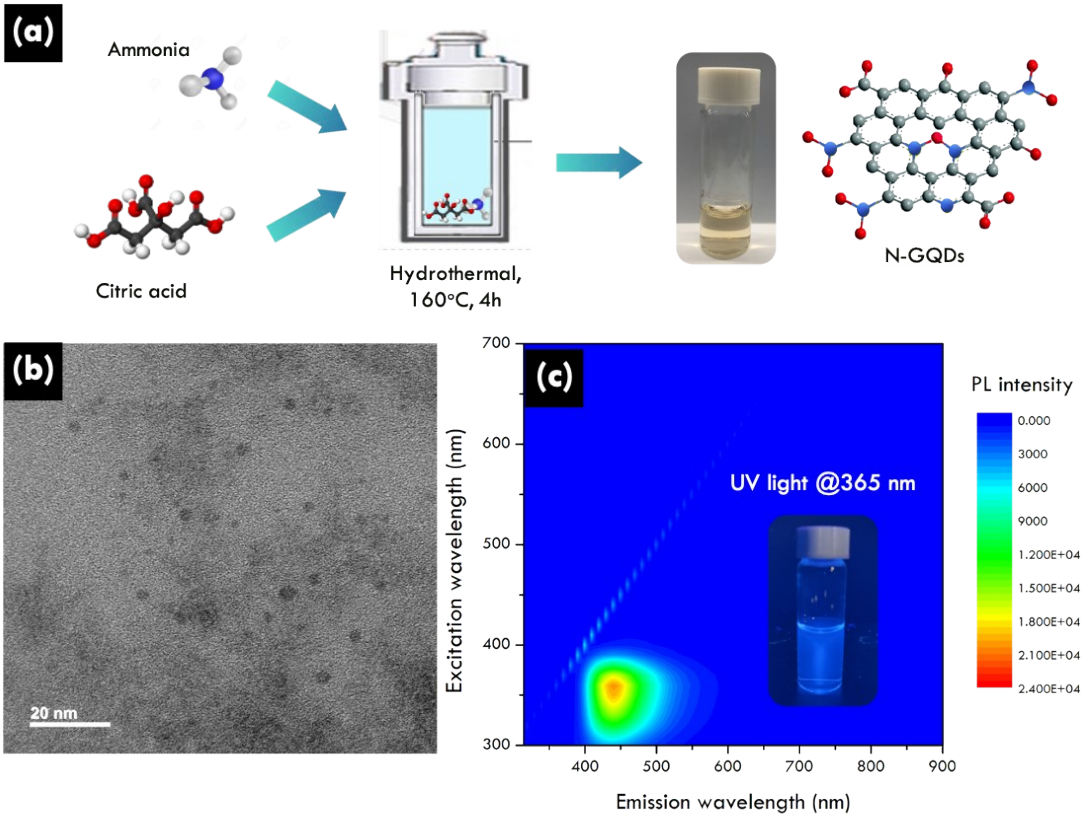

Figure S1 (a). Illustration of the synthesis process of the NGQDs, **(b).** TEM images, and **(c)**. PL excitation-emission-intensity spectra

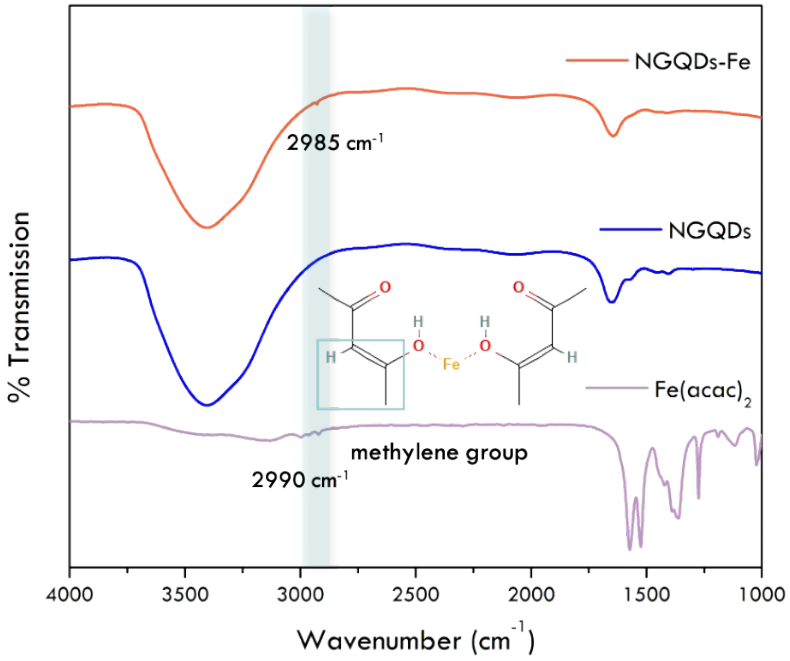

Figure S2 FTIR spectra of NGQDs, $Fe(acac)_2$, and NGQDs-Fe.

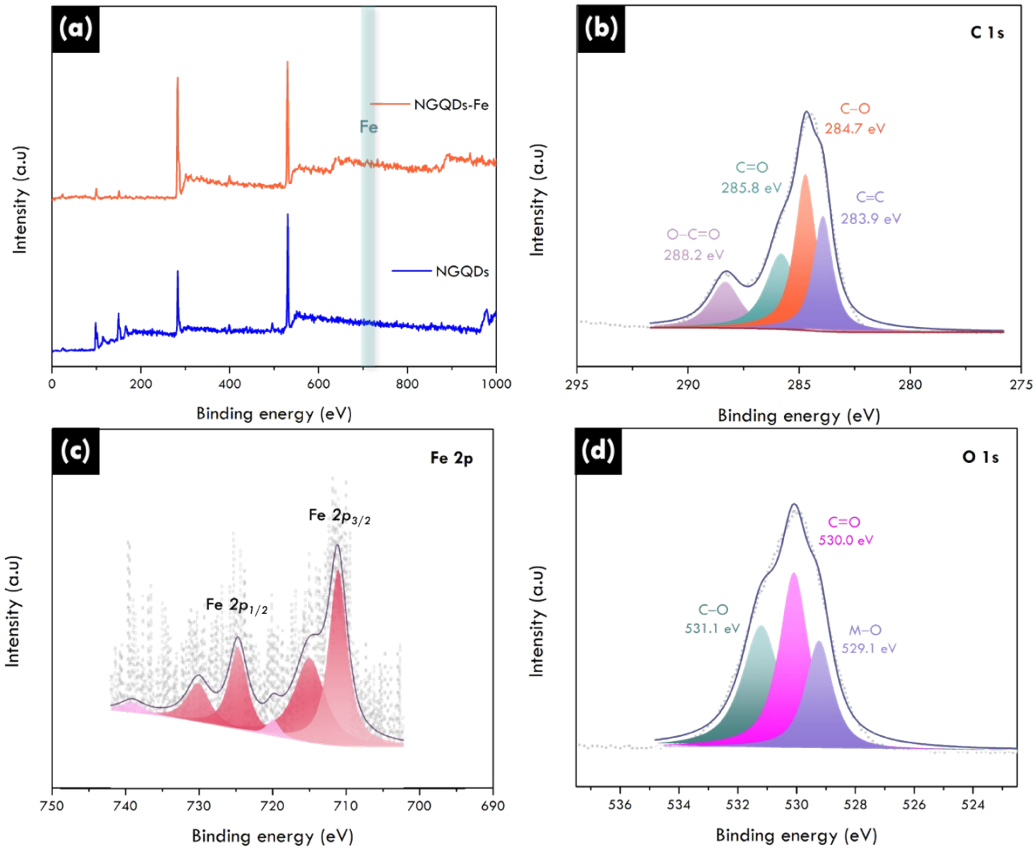

Figure S3 XPS (a). survey scan spectra, and high resolution spectra of (b). C 1s, (c). Fe 2p, and (d). O 1s of NGQDs-Fe

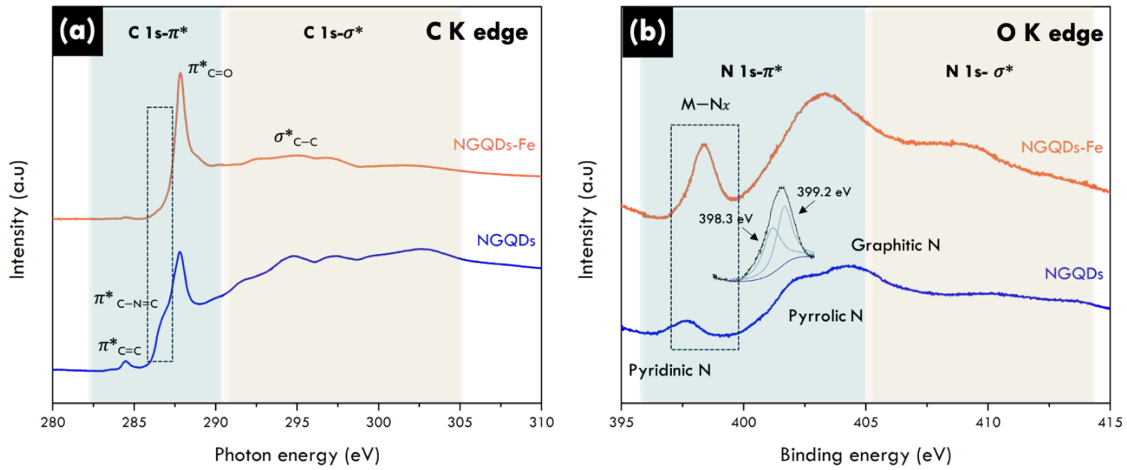

Figure S4. X-ray absorption near-edge structure (NEXAFS) spectra of (a). C K edge and (b). O K edge of NGQDs and NGQDs-Fe

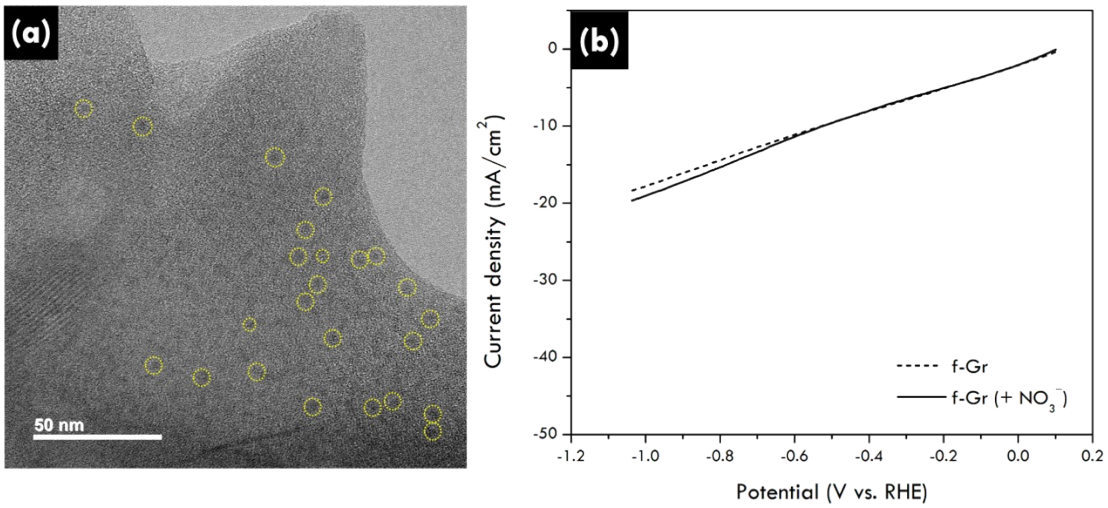

Figure S5 (a). TEM image og NGQDs-Fe, and (c). NO_3^-RR polarization curves of the f-Graphene with and without the presence of the NO_3^- ions.

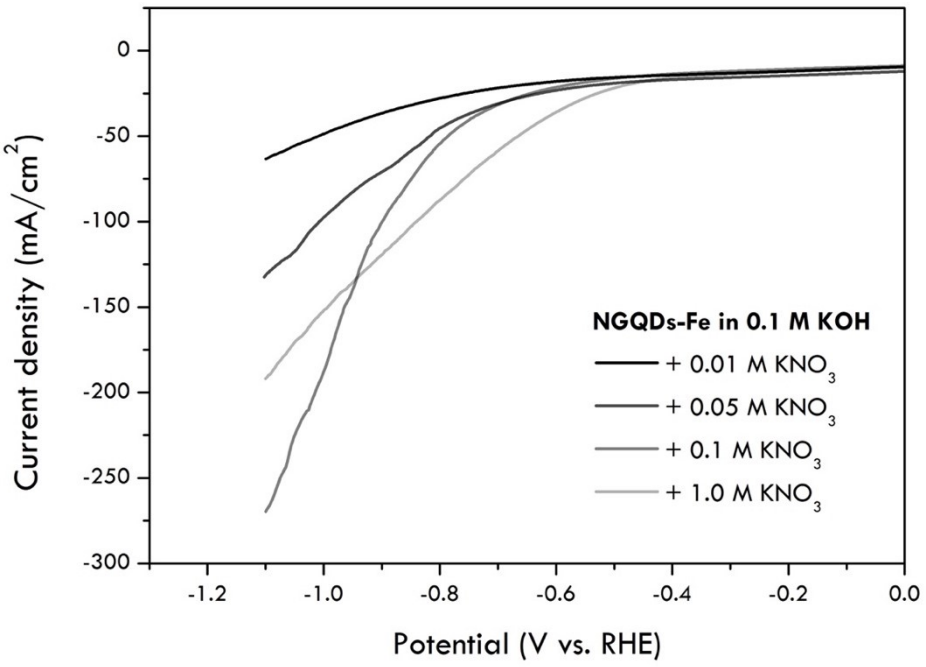

Figure S6 NO_3^- optimization. The polarization curves of the NGQDs-Fe in 0.1 M KOH solution under various KNO_3 concentration.

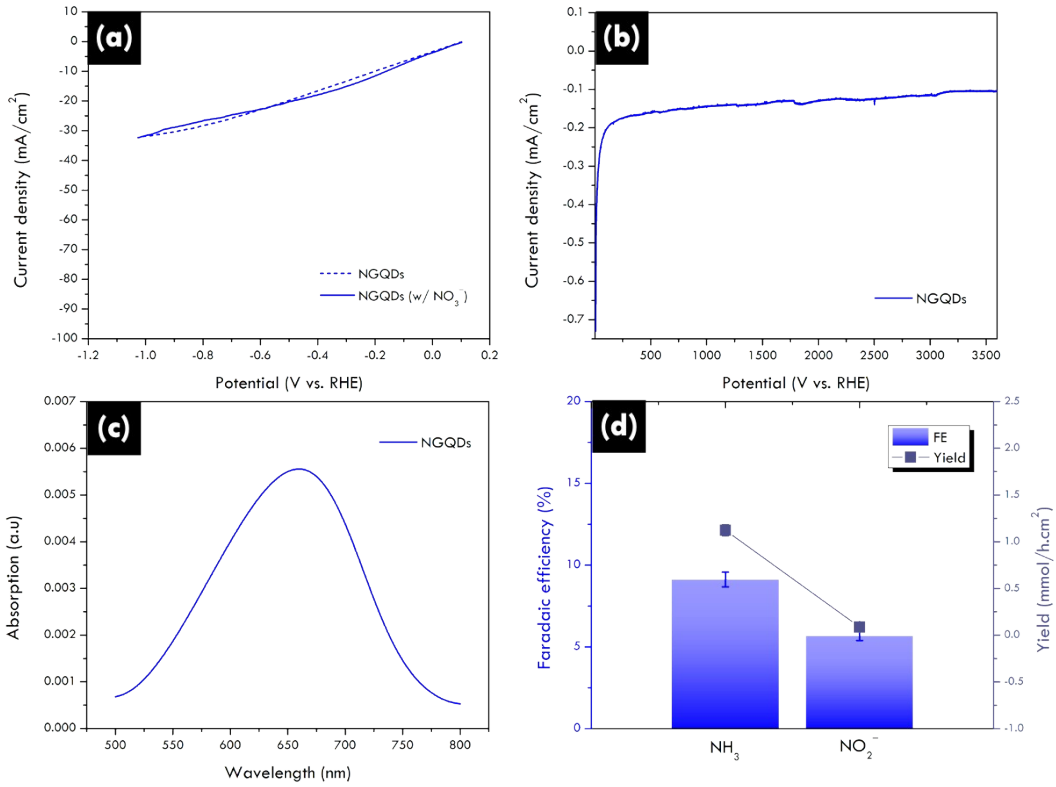

Figure S7 (a). LSV curves of NGQDs with and without the presence of the NO_3^- ions, (b). Chronoamperometry curves at potentials of −0.8 V for 1 h in 0.1 M KOH with 0.1 M NO_3^-, (c). NH_3 UV−Vis absorption spectra of NGQDs, and (d). FE and yield rate of NH_3 and NO_2^-

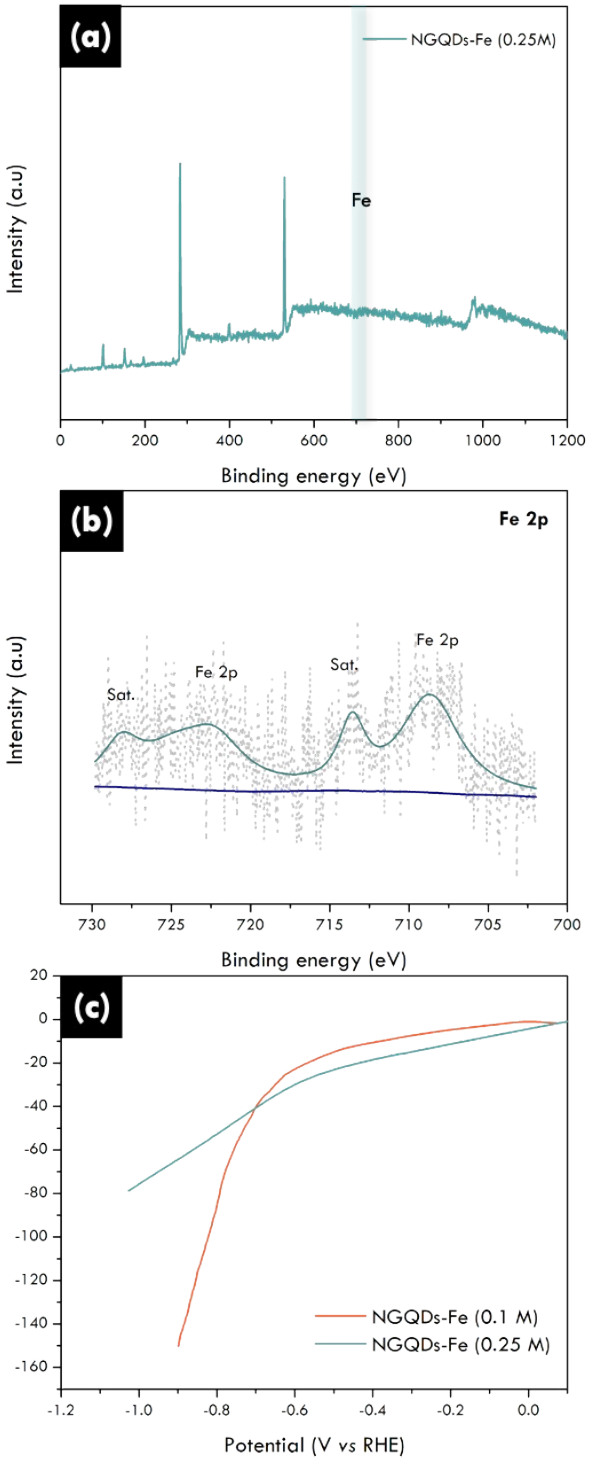

Figure S8 XPS (a). Full-scan spectra, (b). High-resolution spectra of NGQDs-Fe (0.25 M), and (c). LSV curves of the NGQDs-Fe (0.1 M) and (0.25 M) in 0.1 M KOH with 0.1 M NO_3^-

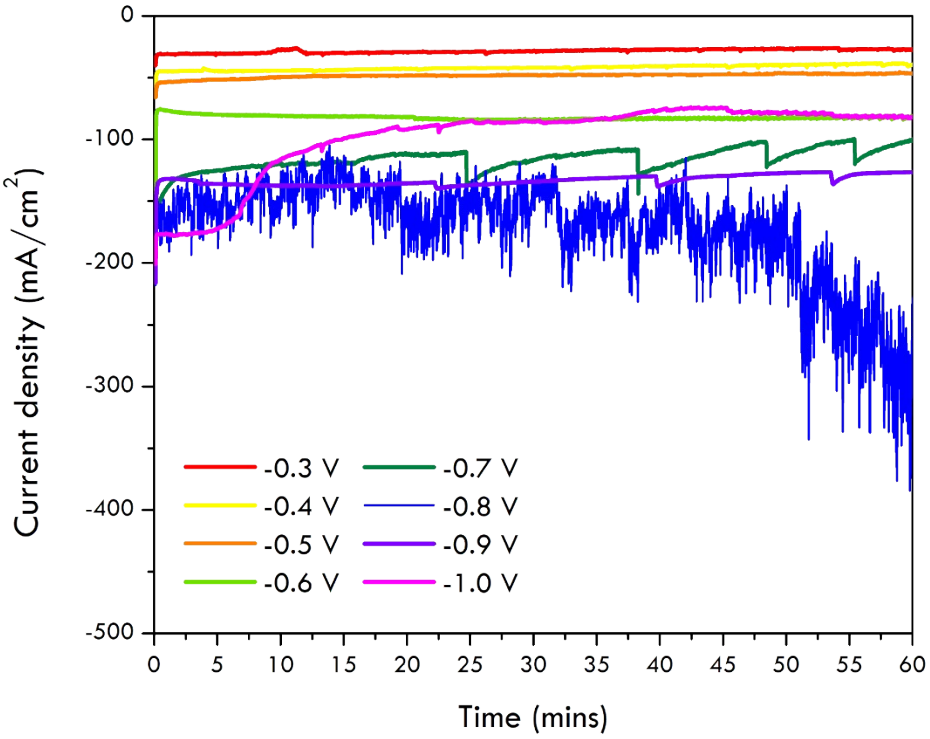

Figure S9 Chronoamperometry curves of NGQDs-Fe across range of potential for 1 h in 0.1 M KOH with 0.1 M NO_3^-

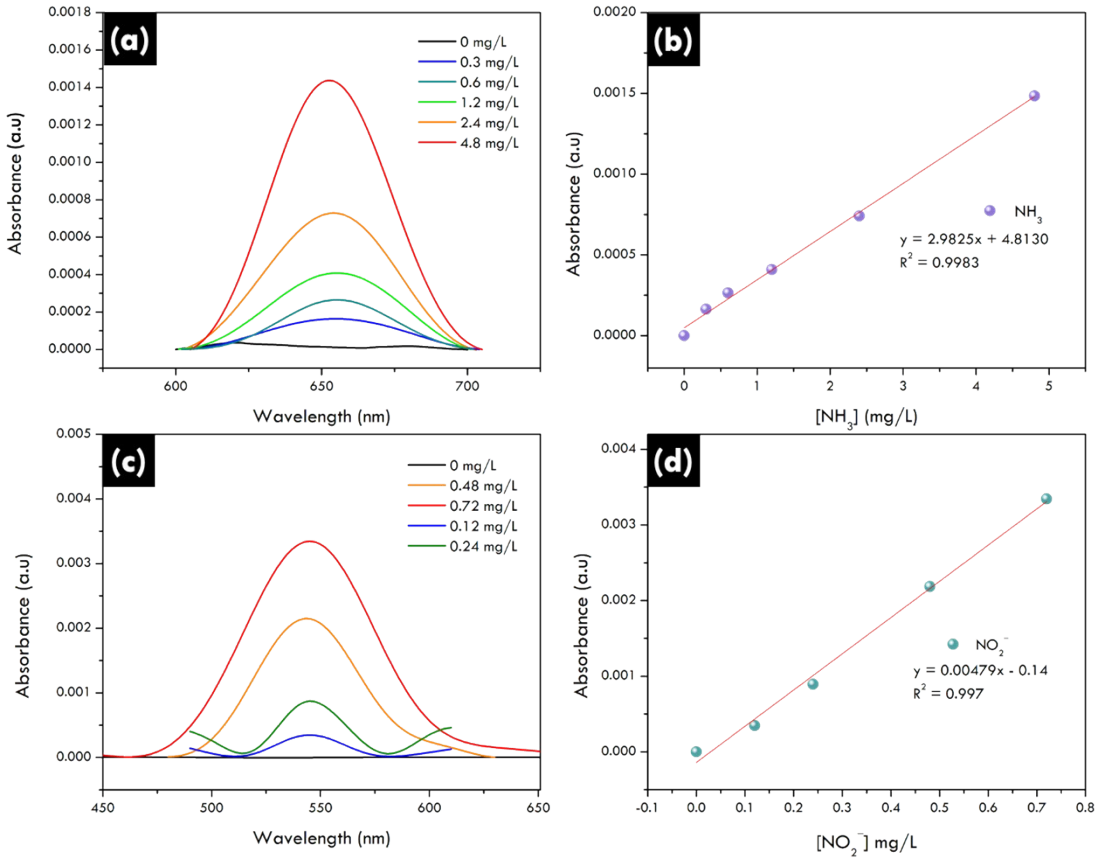

Figure S10 NH_3 and NO_2^- assay using UV-Vis. (a). NH_3 absorption spectra of NH_4Cl in different concentration and (b) corresponding calibration curve for NH_3. (c). NO_2^- absorption spectra of $NaNO_2$ in different concentration and (b) corresponding calibration curve for NO_2^-.

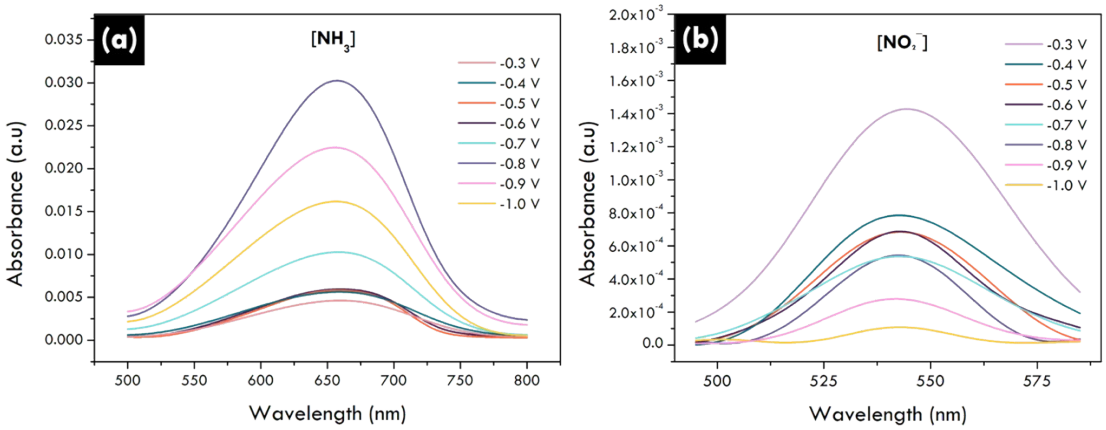

Figure S11 UV-Vis quantification. (a). NH_3 absorption spectra, and (b). NO_2^- absorption spectra of NGQDs-Fe across potential, from −0.3 to −1.0 V.

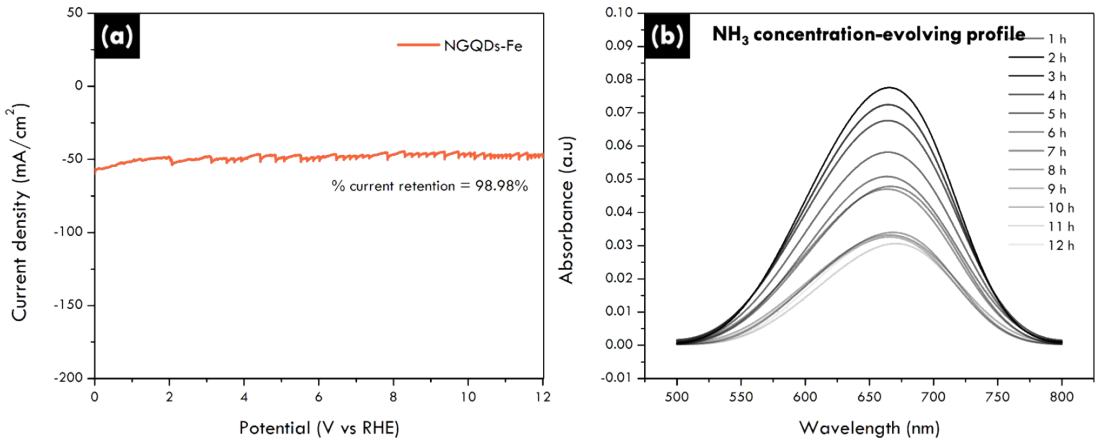

Figure S12 NH_3 concentration evolving profile (a). Chronoamperometry curves of NGQDs-Fe in a continuous cycle in 0.1 M KOH with 0.1 M NO_3^- (b). UV-Vis NH_3 absorption spectra of NGQDs-Fe across cycle

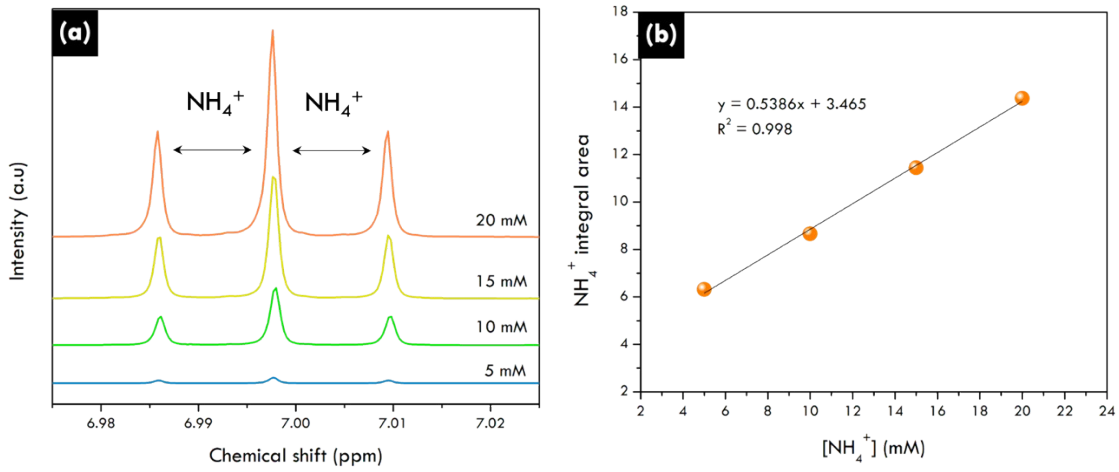

Figure S13 NH_4^+ quantification using NMR (a) ^1H NMR spectra of NH_4^+ ions with different concentrations. Maleic acid (fixed concentration) was used as the external standard, (b). corresponding calibration curves

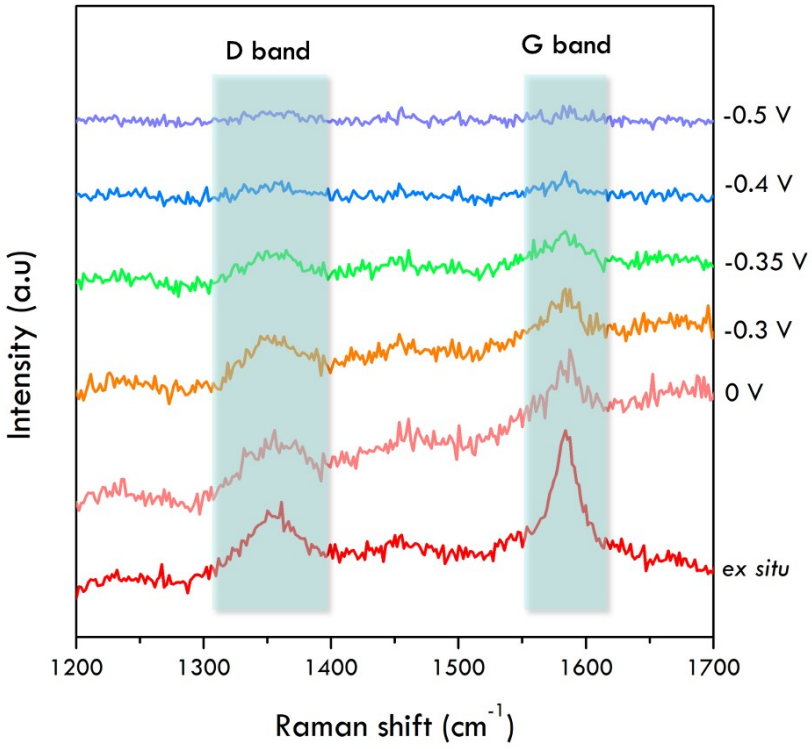

Figure S14 Enlarged *in situ* Raman spectra of the NGQDs-Fe at a different applied potential under 0.1 M of KOH and 0.1 M KNO_3

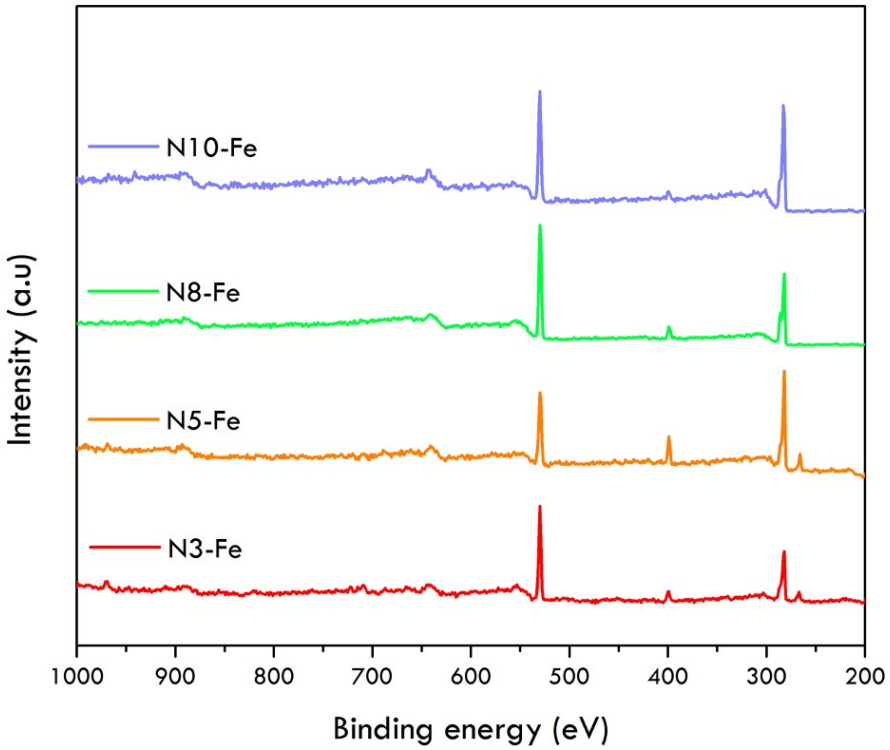

Figure S15. XPS full-scan spectra of the as-synthesized N3-Fe, N5-Fe, N8-Fe, and N10-Fe.

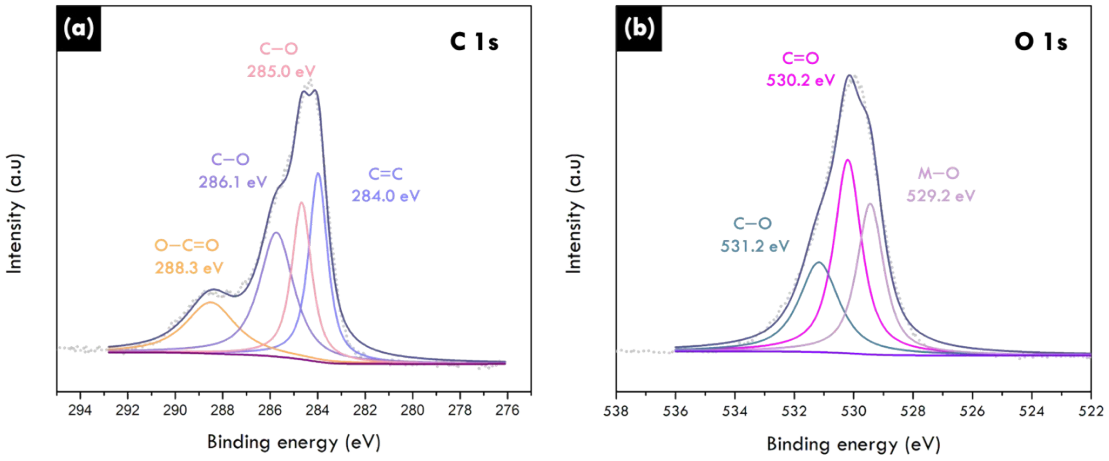

Figure S16. XPS core-level spectra of (a) C 1s, and (b) O 1s of N3-Fe.

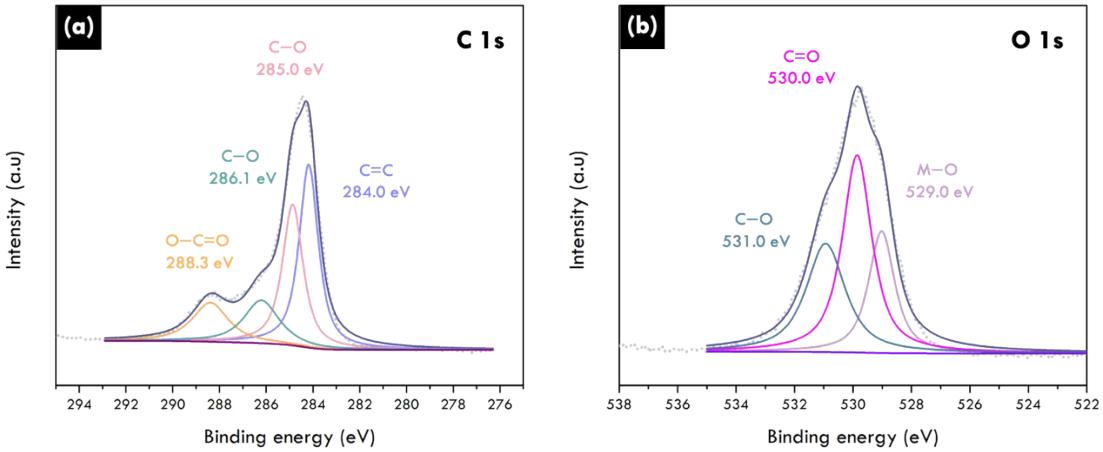

Figure S17. XPS core-level spectra of (a) C 1s, and (b) O 1s of N5-Fe.

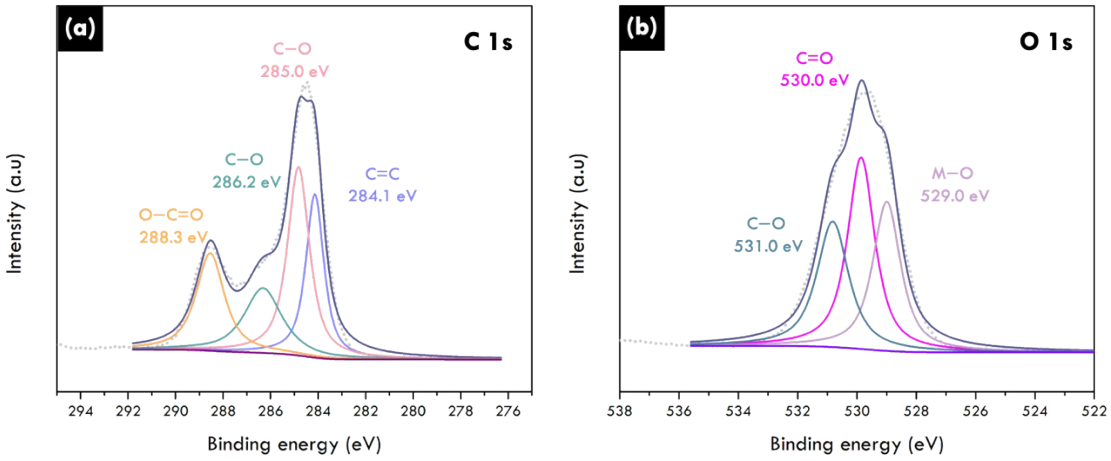

Figure S18. XPS core-level spectra of (a) C 1s, and (b) O 1s of N8-Fe.

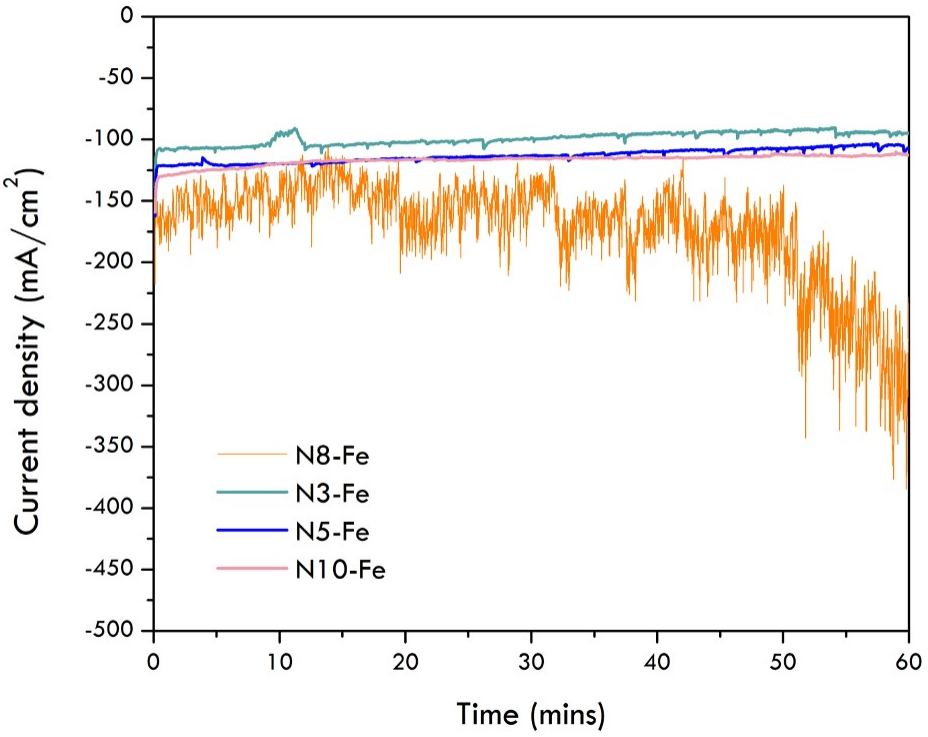

Figure S19 Chronoamperometry curves of the as-synthesized N3-Fe, N5-Fe, N8-Fe, N10-Fe in 0.1 M KOH with 0.1 M NO_3^-

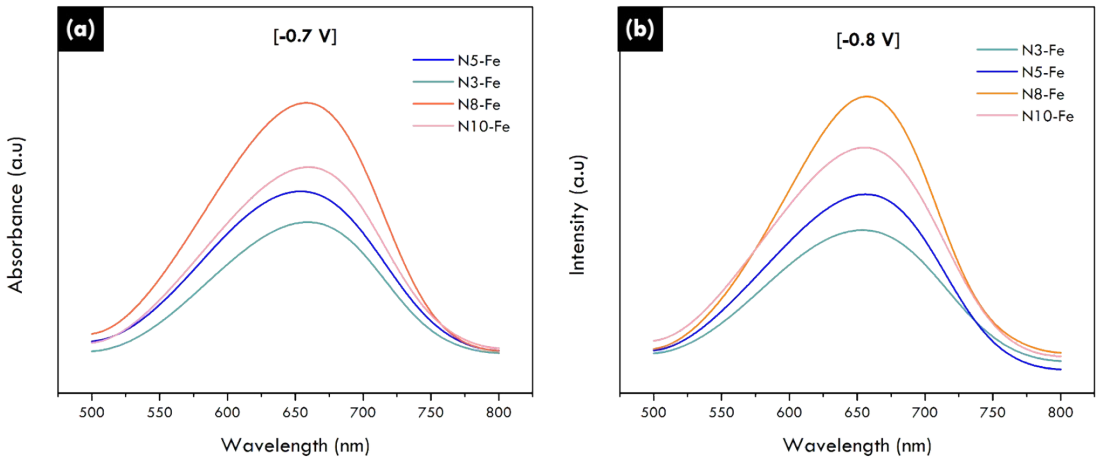

Figure S20 UV-Vis absorption spectra of NH_3 at (a) −0.7 V, and (b). −0.8 V applied potential collected from N3-Fe, N5-Fe, N8-Fe, and N10-Fe.

References

[1] Z.-Y. Wu, M. Karamad, X. Yong, Q. Huang, D.A. Cullen, P. Zhu, C. Xia, Q. Xiao, M. Shakouri, F.-Y. Chen, J.Y. Kim, Y. Xia, K. Heck, Y. Hu, M.S. Wong, Q. Li, I. Gates, S. Siahrostami, H. Wang, Electrochemical ammonia synthesis via nitrate reduction on Fe single atom catalyst, Nature Communications 12(1) (2021) 2870.
[2] Q. Song, M. Li, X. Hou, J. Li, Z. Dong, S. Zhang, L. Yang, X. Liu, Anchored Fe atoms for NO bond activation to boost electrocatalytic nitrate reduction at low concentrations, Applied Catalysis B: Environmental 317 (2022) 121721.
[3] W.-D. Zhang, H. Dong, L. Zhou, H. Xu, H.-R. Wang, X. Yan, Y. Jiang, J. Zhang, Z.-G. Gu, Fe single-atom catalysts with pre-organized coordination structure for efficient electrochemical nitrate reduction to ammonia, Applied Catalysis B: Environmental 317 (2022) 121750.
[4] P. Li, Z. Jin, Z. Fang, G. Yu, A single-site iron catalyst with preoccupied active centers that achieves selective ammonia electrosynthesis from nitrate, Energy & Environmental Science 14(6) (2021) 3522-3531.
[5] Z. Ke, D. He, X. Yan, W. Hu, N. Williams, H. Kang, X. Pan, J. Huang, J. Gu, X. Xiao, Selective NOx– Electroreduction to Ammonia on Isolated Ru Sites, ACS Nano 17(4) (2023) 3483-3491.
[6] S. Zhang, J. Wu, M. Zheng, X. Jin, Z. Shen, Z. Li, Y. Wang, Q. Wang, X. Wang, H. Wei, J. Zhang, P. Wang, S. Zhang, L. Yu, L. Dong, Q. Zhu, H. Zhang, J. Lu, Fe/Cu diatomic catalysts for electrochemical nitrate reduction to ammonia, Nature Communications 14(1) (2023) 3634.
[7] M. Xie, S. Tang, Z. Li, M. Wang, Z. Jin, P. Li, X. Zhan, H. Zhou, G. Yu, Intermetallic Single-Atom Alloy In–Pd Bimetallene for Neutral Electrosynthesis of Ammonia from Nitrate, Journal of the American Chemical Society 145(25) (2023) 13957-13967.
[8] J. Yang, H. Qi, A. Li, X. Liu, X. Yang, S. Zhang, Q. Zhao, Q. Jiang, Y. Su, L. Zhang, J.-F. Li, Z.-Q. Tian, W. Liu, A. Wang, T. Zhang, Potential-Driven Restructuring of Cu Single Atoms to Nanoparticles for Boosting the Electrochemical Reduction of Nitrate to Ammonia, Journal of the American Chemical Society 144(27) (2022) 12062-12071.
[9] Y.-T. Xu, M.-Y. Xie, H. Zhong, Y. Cao, In Situ Clustering of Single-Atom Copper Precatalysts in a Metal-Organic Framework for Efficient Electrocatalytic Nitrate-to-Ammonia Reduction, ACS Catalysis 12(14) (2022) 8698-8706.